J Comput Neurosci
DOI 10.1007/s10827-009-0139-5

Spine neck geometry determines spino-dendritic cross-talk in the presence of mobile endogenous calcium binding proteins

Hartmut Schmidt · Jens Eilers

Received: 15 July 2008 / Revised: 27 January 2009 / Accepted: 29 January 2009

Abstract Dendritic spines are thought to compartmentalize second messengers like Ca^{2+}. The notion of isolated spine signaling, however, was challenged by the recent finding that under certain conditions mobile endogenous Ca^{2+}-binding proteins may break the spine limit and lead to activation of Ca^{2+}-dependent dendritic signaling cascades. Since the size of spines is variable, the spine neck may be an important regulator of this spino-dendritic crosstalk. We tested this hypothesis by using an experimentally defined, kinetic computer model in which spines of Purkinje neurons were coupled to their parent dendrite by necks of variable geometry. We show that Ca^{2+} signaling and calmodulin activation in spines with long necks is essentially isolated from the dendrite, while stubby spines show a strong coupling with their dendrite, mediated particularly by calbindin D28k. We conclude that the spine neck geometry, in close interplay with mobile Ca^{2+}-binding proteins, regulates the spino-dendritic crosstalk.

Keywords Calbindin · Parvalbumin · Kinetic model · Spine · Purkinje neuron

1 Introduction

Spines are femto-liter small protoplasmic protrusions of the dendrites of principal neurons. Their heads carry the postsynaptic specializations of the majority of excitatory synapses and they are connected to the dendritic shaft via a thin, cylindrical neck (Fiala and Harris 2005). Due to their prevalence, it is likely that spines are crucial for brain function. To date, however, their specific roles are controversially discussed with suggestions ranging from mere surface enlargement to significant influences on electrical and/or biochemical signaling (reviewed in Nimchinsky et al. 2002). At present the most common view of spines is that they represent biochemical compartments for second messengers like Ca^{2+} (Gamble and Koch 1987; Zador et al. 1990; Guthrie et al. 1991; Müller and Connor 1991; Koch and Zador 1993; Denk et al. 1995; Svoboda et al. 1996; Sabatini et al. 2002).

Ca^{2+} plays a critical role in the regulation of neuronal excitability and synaptic plasticity. Its cytoplasmic concentration is therefore strictly controlled by endogenous Ca^{2+}-binding proteins (CaBPs) and pumps. Differences in amplitude and time-course of Ca^{2+} transients are thought to determine whether, e.g., strengthening or weakening of synaptic inputs occurs, and biochemical compartmentalization in the spines is thought to underlie these divergent processes (reviewed in Augustine et al. 2003).

Spines, however, vary in their shapes (Spacek and Hartmann 1983; Fiala and Harris 2005). Moreover, the structure of individual spines appears to be dynamically adjusted. Changes in spine shape might be induced rapidly during synaptic activation and plasticity (Crick 1982; Fischer et al. 1998; Bonhoeffer and Yuste 2002; Bloodgood and Sabatini 2005). This raises the possibility that, in the control of Ca^{2+}, the spine neck is a dynamic rather than a static diffusion barrier. Consistent with this notion, recent experimental and theoretical studies suggested an incomplete sequestration of Ca^{2+} in the spine head and a regulation of Ca^{2+} kinetics by the spine neck (Volfovsky et al. 1999; Majewska et al. 2000a, b;

Action Editor: Erik Deschutter

Electronic supplementary material The online version of this article (doi:10.1007/s10827-009-0139-5) contains supplementary material, which is available to authorized users.

H. Schmidt · J. Eilers (✉)
Carl-Ludwig Institut für Physiologie,
Abteilung II, Liebigstr. 27,
04103 Leipzig, Germany
e-mail: jens.eilers@medizin.uni-leipzig.de

Published online: 20 February 2009

Korkotian and Segal 2001; Holcman et al. 2004; Noguchi et al. 2005).

Since experimental observations of Ca^{2+} diffusion are significantly distorted by the use of mobile, fast on-rate Ca^{2+} indicator dyes (Neher 1999; Sabatini et al. 2002), the results from Ca^{2+} imaging experiments are difficult to interpret (Hayashi and Majewska 2005). Yet, the discussion about Ca^{2+} diffusion across the spine neck focused mainly on its contribution in shaping Ca^{2+} kinetics in spines, paying little attention to effects on the dendritic Ca^{2+} homeostasis. Recently, however, we used computer simulations, which were constrained by Ca^{2+}-imaging data from wild-type and CaBP-deficient Purkinje neurons, to show that endogenous CaBPs can shuttle significant amounts of Ca^{2+} into the dendritic shaft (Schmidt et al. 2007). Under the conditions of neighboring co-activated spines and slow synaptic Ca^{2+} signaling, dendritic Ca^{2+} accumulation was sufficient to activate downstream signaling. This form of biochemical signal integration in dendrites exists in parallel and may interact with the dendritic integration of electrical potentials (see Sjöström et al. 2008). In the present study, we investigated whether the spine neck acts as a regulator of dendritic Ca^{2+} summation. Our simulations show that spines with long, thin necks are essentially isolated from their shaft, while those with short, thick necks show an intense spino-dendritic coupling mediated by the endogenous CaBPs calbindin D-28k and, to a lesser extent, parvalbumin.

2 Methods

2.1 Fluorescence recordings

Ca^{2+} imaging experiments were performed on spiny dendrites of Purkinje neurons (PNs) in acute cerebellar slices of 21- to 24-day-old C57Bl6 mice as described previously (Schmidt et al. 2003a, 2007). Briefly, PNs were equilibrated in the whole-cell patch-clamp configuration with an indicator dye-containing pipette solution of the following composition (in mM): 140 K-gluconate, 10 NaCl, 3 Mg-ATP, 0.3 GTP, 10 HEPES; 0.2 or 0.1 Oregon Green 488 BAPTA-1 (OGB, Invitrogen, Carlsbad, CA, USA) dissolved in purified water (W-3500, Sigma, Munich, Germany). The pH was adjusted to 7.3 (at 19–21°C) with KOH. Experiments were performed 60 to 120 min after the whole-cell configuration was established, a time period in which the dendritic dye concentration reached 70% to 80% of that in the pipette solution (Rexhausen 1992). The ACSF contained (in mM): 125 NaCl, 2.5 KCl, 1.25 NaH_2PO_4, 26 $NaHCO_3$, 1 $MgCl_2$, 1.8 $CaCl_2$, 20 glucose, pH 7.3 to 7.4 at 19–21°C when gassed with 95% O_2 and 5% CO_2.

Synaptic Ca^{2+} transients were elicited by stimulating afferent climbing or parallel fibers (CFs and PFs, respectively). The corresponding fluorescence signals were recorded with a confocal laser-scanning microscope (Fluoview-300, Olympus) equipped with a 60×/0.9 N.A. water immersion objective in the line-scan mode at a sampling rate 2 ms per line. Metabotropic Ca^{2+} signals (Takechi et al. 1998; Finch and Augustine 1998) were evoked by burst stimulation of PFs (3 to 5 stimuli given at 20 to 50 Hz) in the presence of the AMPA (α-amino-3-hydroxy-5-methyl-isoxazole-4-propionic acid) receptor antagonist CNQX (6-cyano-7-nitroquinoxaline-2,3-dione, 30 to 50 μM, Sigma, Munich, Germany). Only spines that were clearly discriminable from the adjacent dendrite were accepted for analysis.

2.2 Data analysis

Fluorescence data were expressed as $\Delta F/F_0$ (i.e., as background-corrected fluorescence increase divided by the baseline fluorescence) and filtered using a sliding average of nine points ('box filter' Igor Pro). $\Delta F/F_0$ values were converted to free Ca^{2+} concentrations ($[Ca^{2+}]_{free}$) based on five independent cuvette calibrations in our pipette solution (Schmidt et al. 2003a), using a commercial calibration kit (C-3723, Invitrogen) and custom-written routines in Igor Pro 5.0 (Wavemetrics, Lake Oswego, OR, USA) to fit the following formula to the data:

$$F = \left(\left([Ca^{2+}]_{free}/K_D\right)F_{max} + F_{min}\right)/\left(1 + [Ca^{2+}]_{free}/K_D\right) \quad (1)$$

where F_{min} and F_{max} is the fluorescence at 0 and 20 μM $[Ca^{2+}]_{free}$, respectively. This fit yielded an indicator K_D of 325 nM and, assuming a resting $[Ca^{2+}]$ of 45 nM (Wilms et al. 2006), was used to convert $\Delta F/F_0$ values to $[Ca^{2+}]_i$.

The decay of each CF-induced Ca^{2+} transient was fitted with a double-exponential function of the form

$$[Ca^{2+}]_i = [Ca^{2+}]_{rest} + A_1 e^{-\left(\frac{t}{\tau_1}\right)} + A_2 e^{-\left(\frac{t}{\tau_2}\right)} \quad (2)$$

where $[Ca^{2+}]_{rest}$ is the assumed resting $[Ca^{2+}]_i$ of 45 nM, $A_{1,2}$ and $\tau_{1,2}$ the amplitudes, and decay time constants of two decay components. For each metabotropic PF-mediated transient the complete waveform (rise and decay) was fitted with a modified α function of the form

$$[Ca^{2+}]_i = \begin{cases} [Ca^{2+}]_{rest} & \text{if } t < t_0 \\ [Ca^{2+}]_{rest} + e^{-\left(\frac{t-t_0}{\tau_{decay}}\right)} - e^{-\left(\frac{t-t_0}{\tau_{rise}}\right)} \end{cases} \quad (3)$$

where τ_{rise} and τ_{decay} are the time constants of the rising and decay phase, respectively.

From the obtained fit parameters, median spineous and dendritic transients were calculated, that represented "rapid" signals (CF-evoked transients, with Ca^{2+} influx through voltage-gated Ca^{2+} channels and/or ionotropic glutamate receptor channels) or "slow" signals (PF-mediated activation of metabotropic glutamate receptors with IP3-mediated Ca^{2+} release).

2.3 Kinetic two-compartment model

Ca^{2+} transients were simulated as described previously (Schmidt et al. 2003a, 2007) by numerically solving a system of ordinary differential equations (ODEs) using Mathematica 5.0 (Wolfram Research, Champaign, IL, USA). The ODEs covered a surface based Ca^{2+} influx, binding of Ca^{2+} to the fast and slow binding sites of calbindin D-28 k (CB), to parvalbumin (PV), and, as indicated, to calmodulin (CaM), binding of Mg^{2+} to PV, diffusion of all species, and a surface based clearance mechanism with Michaelis–Menten kinetics. The model described a spine and its parent dendrite, optionally coupled by diffusion. As indicated, the spine geometry was set to either reflect the mean spine geometry or that of "stubby" or "slim" spines (Fig. 1; Harris and Stevens 1988; Vecellio et al. 2000). The length of the dendritic compartment was set to 0.3 µm. Given the spine density of distal dendrites (three to four spines/µm), this value reflects the situation in which neighbouring spines are coactive and, therefore, net diffusional exchange for each spine can be simplified as exchange with its small parent dendritic compartment (Schmidt et al. 2007).

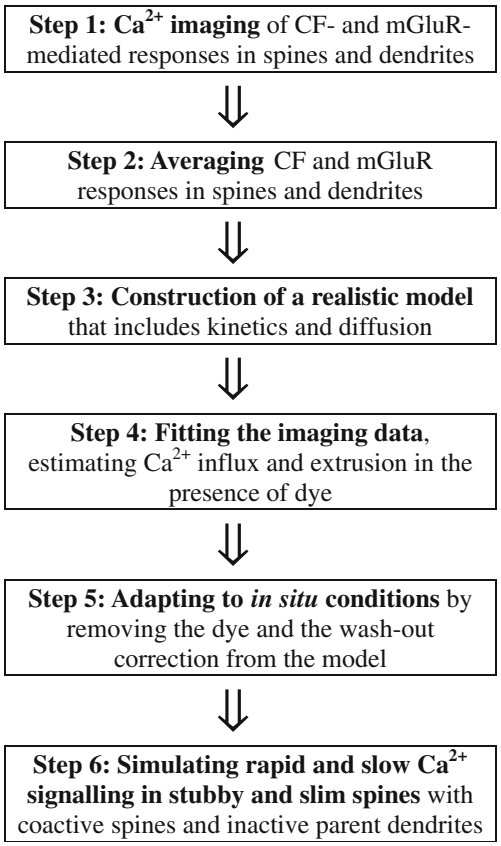

Fig. 1 Outline of the combined experimental and numerical approach. *CF* climbing fiber, *mGluR* metabotropic glutamate receptors

The Ca^{2+} influx (I_{Ca}) during CF stimulation ("rapid" signal, Fig. 2(a–c)) was represented by

$$I_{\mathrm{Ca,\,rapid}} = I_0 e^{-\left(\frac{t-t_0}{\sigma}\right)^2} \tag{4a}$$

where I_0 denotes the maximal amplitude of the current which is reached at t_0 and σ is the width of the function. The mGluR-mediated Ca^{2+} increase ("slow" signal, Fig. 2(d)) was represented by an α function that allowed for separate adjustment of the rising and decay phase:

$$I_{\mathrm{Ca,\,slow}} = I_0 \left(e^{-\left(\frac{t-t_0}{\tau_{\mathrm{decay}}}\right)} - e^{-\left(\frac{t-t_0}{\tau_{\mathrm{rise}}}\right)} \right) \tag{4b}$$

The increase in $[Ca^{2+}]_i$ caused by the Ca^{2+} influx is given by

$$\left(\frac{\mathrm{d}\left[Ca^{2+}\right]}{\mathrm{d}\,t}\right)_{\mathrm{influx}} = \frac{A I_{\mathrm{Ca}}}{2FV} \tag{5}$$

where A is the surface of the spine or dendrite, respectively, F is Faraday's constant, and V the volume of the compartment.

Ca^{2+} binding to OGB, CB, PV, and CaM was simulated assuming second order kinetics for all reactions. The four binding sites of CB and the two binding sites of PV were simulated as individual reaction partners, neglecting possible cooperativity. For CaM only one of the four binding sites was simulated with the rate-limiting kinetics of the first Ca^{2+} binding step (Sabatini et al. 2002). In view of the lack of information about the intracellular CaM concentration in PNs, we adhered to the commonly used value of 10 µM (Keller et al. 2008; Sabatini et al. 2002), which, given the affinity of CaM and the prevalence of CB and PV, can be expected not to disturb the simulated Ca^{2+} dynamics (Neher 1999). Under these assumptions, the rate of change in $[Ca^{2+}]_i$ due to binding of Ca^{2+} to the j-th binding site (BS_j) is given by

$$\left(\frac{\mathrm{d}\left[Ca^{2+}\right]}{\mathrm{d}\,t}\right)_{\mathrm{buffer},j} = -k_{on,j}\left[Ca^{2+}\right]\left[BS_j\right] + k_{\mathrm{off},j}\left[CaBS_j\right] \tag{6}$$

$j = 1$ for OGB
$j = 2-5$ for CB
$j = 6, 7$ for PV
$j = 8$ for CaM

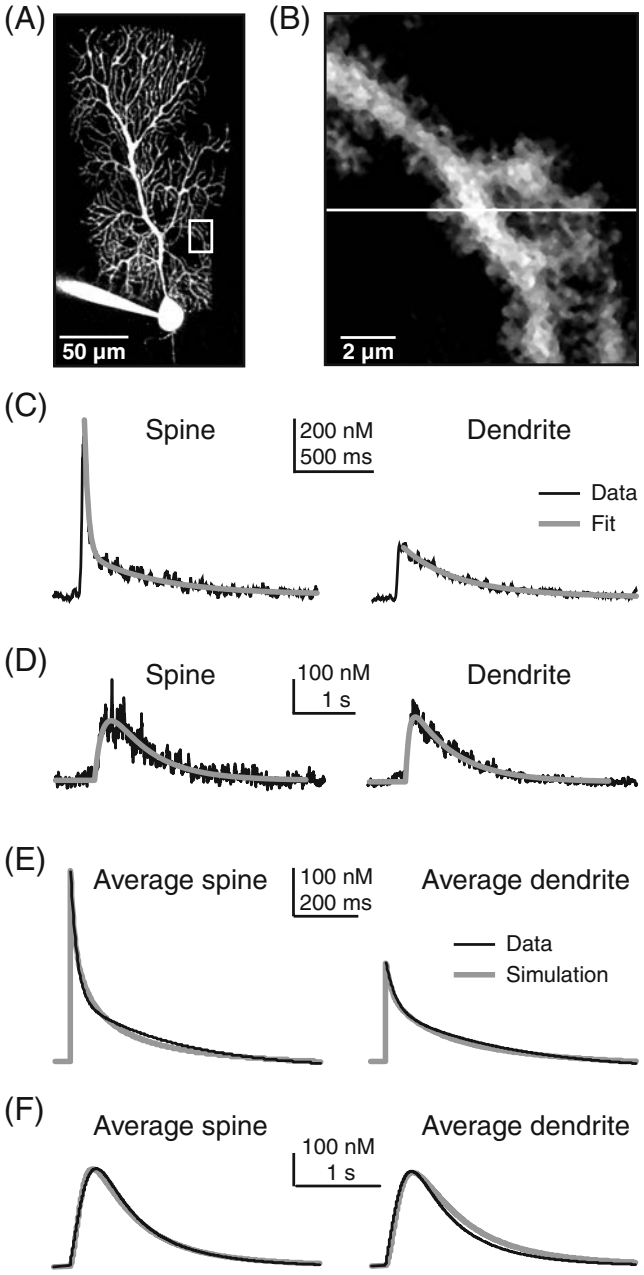

◀ **Fig. 2** Rapid and slow postsynaptic Ca^{2+}-signals in Purkinje neurons. (**a**) Contrast-enhanced image of a Purkinje neuron in an acute cerebellar slice, loaded with the Ca^{2+} indicator dye Oregon Green 488 BAPTA-1 (OGB, 80 µM) via a somatic whole-cell patch-pipette (*lower left*) for 1 h. (**b**) Higher magnification of the dendritic region outlined in A. The *white line* indicates the region of interest (ROI) from which fluorescence signals during CF-activation were recorded in the line-scan mode. (**c**) CF-fiber mediated Ca^{2+} signals in the spine (*left*) and in the dendrite (*right*) from the ROI shown in (**b**). The *gray lines* represent double-exponential fits to the data. (**d**) Ca^{2+} signals elicited by burst stimulation of afferent parallel fibers (PF) in the presence of the AMPA-receptor antagonist CNQX. Ca^{2+} signals were fitted (*gray line*) with a modified α function that allowed for independent adjustment of the rise and decay time constants. Recording from a different cell than in (**a**–**c**). (**e**) Median Ca^{2+} transients (*black lines*) measured in spines and dendrites (*left and right columns*, respectively; n=252) during CF stimulation and the corresponding fits (*gray lines*) of the kinetic model. (**f**) As in (**e**) but for Ca^{2+}-signals evoked by PF burst stimulation (n=66)

For OGB, CB, and CaM the following relationship between changes in free (BS_j) and Ca^{2+}-occupied binding sites ($CaBS_j$) applies:

$$\left(\frac{d[BS_j]}{dt}\right) = -\left(\frac{d[CaBS_j]}{dt}\right) \quad j = 1-5, 8 \tag{7}$$

For PV the situation is complicated by its medium affinity for Mg^{2+} which significantly affects its Ca^{2+}-binding kinetics. The change in the occupancy of PV's binding sites is given by

$$\left(\frac{d[BS_j]}{dt}\right) = -\left(\frac{d[CaBS_j]}{dt}\right) - \left(\frac{d[MgBS_j]}{dt}\right) \tag{8}$$

$$j = 6, 7$$

and

$$\left(\frac{d[Mg^{2+}BS_j]}{dt}\right) = -k_{on,j,Mg}[Mg^{2+}][BS_j] + k_{off,j,Mg}[MgBS_j] \qquad j = 6, 7 \tag{9}$$

The intracellular Mg^{2+} concentration was held constant at 590 µM, the value calculated for our pipette solution using WinMaxC 2.1 software (http://www.stanford.edu/~cpatton/maxc.html). The starting conditions were calculated from chemical equilibrium at $[Ca^{2+}]_{rest}$.

A single Ca^{2+} extrusion mechanism was simulated assuming Michaelis–Menten kinetics:

$$\left(\frac{d[Ca^{2+}]}{dt}\right)_{pump} = -v_{max}\frac{A}{V}\left(\frac{[Ca^{2+}]}{[Ca^{2+}]+K_M}\right) \tag{10}$$

where K_M is the Michaelis–Menten constant and v_{max} the maximal pump velocity. K_M was set high enough (3 µM) to yield a linear extrusion rate for the observed Ca^{2+} transients. In order to establish the resting $[Ca^{2+}]_i$, the Ca^{2+} clearance was balanced by a leak current:

$$\left(\frac{d[Ca^{2+}]}{dt}\right)_{leak} = v_{max}\frac{A}{V}\left(\frac{[Ca^{2+}]_{rest}}{[Ca^{2+}]_{rest}+K_M}\right) \tag{11}$$

For a given molecular species X, the diffusional current J_X across the spine neck was simulated as

$$J_X = D_X \frac{\pi r_{\text{neck}}^2}{l_{\text{neck}}} \left(C_{X,\text{spine}} - C_{X,\text{ dendrite}}\right) \quad (12)$$

where D_X and C_X are the diffusion coefficient and the concentration of the diffusing species, respectively, and r_{neck} and l_{neck} are the radius and the length of the spine neck. The rate of change in the concentration of X due to diffusion follows as

$$\left(\frac{\mathrm{d}[X]}{\mathrm{d}t}\right)_{\text{diffusion}} = -\frac{J_X}{V_{\text{spine}}} \quad (13a)$$

for the spine and

$$\left(\frac{\mathrm{d}[X]}{\mathrm{d}t}\right)_{\text{diffusion}} = \frac{J_X}{V_{\text{dendrite}}} \quad (13b)$$

for the dendrite. The simulation included independent diffusion of the free binding sites of OGB, CB, PV, and CaM, of the corresponding Ca^{2+}-bound binding sites, of the Mg^{2+}-bound binding sites of PV, and of free Ca^{2+}. The time course of the total change in $[Ca^{2+}]_i$ is given by the sum of Eqs. (4)–(13). *Mathematica* source files are provided as supplemental material.

2.4 Fitting the model to the data

Most parameters for the above equations could be obtained from the literature or were defined by the experimental conditions, see Appendix. The cytosolic concentration of the endogenous proteins CB and PV were reduced to correct for the wash-out occurring during the prolonged whole-cell recording (Rexhausen 1992; Müller et al. 2005). Spine parameters were chosen to reflect the mean spine geometry (Harris and Stevens 1988; Vecellio et al. 2000). First, CF-mediated Ca^{2+} transients were fitted, with the Ca^{2+} influx parameter I_0 (Eq. (4a)) and $v_{\max}$ of the extrusion (Eq. (10)) as the only free variables. Subsequently, $v_{\max}$ was held constant and mGlu-mediated transients were fitted with the Ca^{2+} influx parameters I_0, τ_{decay} and τ_{rise} (Eq. (4b)) as free variables. Variables were adjusted manually until the simulations yielded a maximal overlap with the median Ca^{2+} transients recorded in spines and dendrites.

2.5 Modeling of spineous Ca^{2+} signals

With influx and extrusion parameters obtained from fits to the measurements, the now fully defined model was adapted to reflect rapid and slow spine Ca^{2+} signals in the unperturbed *in situ* condition: the dye was omitted from the simulation, the naïve concentrations (without wash-out correction) of CB and PV were used, and the Ca^{2+} influx was restricted to the spines. Two different spine neck geometries were simulated, a short neck with a large "effective" (i.e. corrected for the contribution of the ER) diameter ("stubby" spines), and a long neck with a small effective diameter ("slim" spine; Harris and Stevens 1988; Vecellio et al. 2000).

3 Results

3.1 Synaptically induced Ca^{2+} signals in spiny dendrites

Cerebellar Purkinje cells (PNs) respond to synaptic excitation with two main Ca^{2+} signaling patterns (Hartmann and Konnerth 2005), (1) rapid signals mediated by activation of ionotropic glutamate receptors (iGluRs) and/or voltage-gated calcium channels (VOCCs) and (2) slow signals mediated by metabotropic glutamate receptors (mGluRs). Rapid Ca^{2+} signals are reliably evoked by stimulation of the afferent climbing fiber (CF), which depolarizes the PN above threshold and generates widespread dendritic Ca^{2+} signals. Figure 2(a–c) shows CF-mediated Ca^{2+} transients in a PN loaded with the high-affinity Ca^{2+} indicator dye OGB. In agreement with previous studies (Schmidt et al. 2003a), the spineous transients reached peak amplitudes of 415 (307–609) nM and showed a bi-exponential decay with time constants in the range of 20 (13–30) and 330 (281–384) ms (median and interquartile range, n=252). Similar time constants were found in the accompanying dendrites, the amplitudes, however, were significantly smaller (262 (171–351) nM; Fig. 2(c)), mostly due to a reduction of the fast component (comp. Schmidt et al. 2003a).

Slow synaptic Ca^{2+} transients were induced by burst stimulation of the afferent parallel fibers (PFs, Fig. 2(d)). The waveform of the transient was well fitted by an α function with independent rise and decay time constant. Compared to the CF responses, the slow transients showed a greater variability between recordings (Takechi et al. 1998; Finch and Augustine 1998; Barski et al. 2003). For a given recording, however, spines and dendrites showed similar amplitudes (351 (274–490) nM and 329 (272–475) nM; n=79 spines and 66 dendrites) as well as comparable rise and decay time constants (180 (92–205) and 490 (390–536) ms in spines and 179 (90–217) and 510 (405–532) ms in dendrites).

The variable morphology of spines and dendrites can be expected to significantly contribute to the variability of the Ca^{2+} responses (Noguchi et al. 2005). Most morphological parameters of PN spines and dendrites show a skewed distribution (Vecellio et al. 2000). Similarly, the Ca^{2+} signals showed a non-Gaussian distribution and, therefore, median fit values were used to calculate average spineous and dendritic Ca^{2+} transients (Fig. 2(e, f)).

3.2 A reaction-diffusion model describes rapid and slow Ca^{2+} transients in spines and dendrites

The measured Ca^{2+} signals served as templates for our simulations of spino-dendritic Ca^{2+} signaling. We had previously shown that a reaction-diffusion model (see Section 2) well describes rapid Ca^{2+} signals in spiny dendrites (Figure 2(e) and Schmidt et al. 2003a, 2007) Fig. 2(f) shows that the same model, with all parameters held constant but the amplitude and the time constants of the Ca^{2+} influx, also faithfully describes the slow transient in both compartments, the spine as well as the dendrite.

The robustness of this model, which also describes Ca^{2+} kinetics in mutants that lack the endogenous Ca^{2+}-binding proteins calbindin D28k (CB) or CB and parvalbumin (PV; Schmidt et al. 2007), allowed the analysis of unperturbed spino-dendritic Ca^{2+}-signaling under experimentally constrained conditions. For this purpose the Ca^{2+} influx and extrusion parameters, as derived from the above fits, were set as constants, and the indicator dye and the wash-out correction for CB and PV were removed from the simulations. Subsequently, the influx was omitted form the dendrite and the spine geometry was varied (Fig. 1 and Section 2).

3.3 Rapid Ca^{2+} signaling in stubby and slim spines

We continued by analyzing fast Ca^{2+} signals occurring in spines (Denk et al. 1995). Specifically, we quantified to what extent the diffusional exchange between the spine and its parent dendrite is affected by the spine morphology. Figure 3 illustrates the modeled dynamics in stubby and slim spines that correspond to the measured median Ca^{2+} transient, supplemental Fig. 1 shows the same analysis also for the upper and lower bounds of Ca^{2+} transients, i.e. for the interquartile range signals.

In the stubby spine, the free intracellular Ca^{2+} concentration ($[Ca^{2+}]_i$) during the average Ca^{2+} transient reached about 1.8 μM for a few ms before it rapidly decayed back to the resting level of 45 nM (Fig. 3(A1)). In total, 4,700 calcium ions entered the spine during the simulated transient. In the inactive dendrite, diffusional flux increased $[Ca^{2+}]_i$ only by 10–20 nM (inset). During the transient neither PV (which, in the presence of physiological concentrations of Mg^{2+}, binds Ca^{2+} rather slowly, (Lee et al. 2000a; Schmidt et al. 2003a) nor the slow binding sites of CB (CB_{slow}) bound significant amounts of Ca^{2+}. Only the fast binding sites of CB (CB_{fast}) could capture Ca^{2+} during the transient (Fig. 3(B1)).

The spineous increase in free Ca^{2+} and Ca^{2+}-bound CB drove a pronounced but brief diffusional net transport of Ca^{2+} out of the spine (Fig. 3(C1)). In total, more than 80% of the spineous Ca^{2+} load left the spine via the neck: > 70% bound to CB and > 10% as free Ca^{2+}. Buffered transport by PV was negligible. Despite the strong Ca^{2+} efflux from the spines, the dendritic free Ca^{2+} concentration was only slightly affected (see above) and also the concentration of Ca^{2+}-bound PV and CB did not change significantly (Fig. 3(D1)). The subtle changes in the dendrite are readily explained by the large volume difference between spine and dendrite, which minimizes the dendritic impact of short-lived Ca^{2+} efflux from the spine (Schmidt et al. 2007). Taken together, the short, thick necks of stubby spines mediate a strong diffusional coupling to the parent dendrite that shapes spineous Ca^{2+}-decay kinetics but only slightly affects the dendritic Ca^{2+} homeostasis. These findings apply to all three simulated Ca^{2+} transients, with little differences between the median transient and those that correspond to the smaller and larger transients defined by the interquartile ranges of the measured Ca^{2+} responses (Fig. S1).

Slim spines showed markedly different Ca^{2+} dynamics (Fig. 3, right column). While the peak amplitude of $[Ca^{2+}]_i$ was only slightly increased to ~2 μM on average, the transient showed a pronounced biphasic decay (Fig. 3(A2)). Ca^{2+} complexation by PV and the fast and slow binding sites of CB was significantly increased and prolonged (Fig. 3(B2)). Despite the higher concentration and longer availability of diffusing species (Fig. 3(B2)), the efflux through the thin spine neck was strongly reduced. The flux per ms was reduced by two orders of magnitude (Fig. 3(C2)) and its temporal integral (inset) was only ~39% of the efflux occurring in stubby spines. The majority of the Ca^{2+} flux, corresponding to ~38% of the spineous Ca^{2+} load, was carried by CB and PV. Diffusion of free Ca^{2+} was negligible (<1%). Neither the dendritic $[Ca^{2+}]_i$ nor the concentration of Ca^{2+}-bound PV or CB were altered by the long-lasting diffusional exchange (Fig. 3(A2)) inset and D2).

In order to estimate the degree of compartmentalization mediated by the neck of slim spines, we excluded diffusion between spine and shaft from the model. The resulting spineous Ca^{2+} transient was nearly indistinguishable from that in the slim spine with diffusional coupling to the dendrite (data not shown). In addition, the time-course and degree of CB and PV occupancy were almost identical under both conditions. Thus, during rapid synaptic Ca^{2+} signaling, slim spines are functionally isolated from their shaft, even in the presence of large amounts of mobile endogenous CaBPs.

3.4 Slow Ca^{2+} signaling

We next analyzed the impact of spine geometry on slow synaptic Ca^{2+} signals such as those occurring during activation of metabotropic glutamate receptors (mGluR; Finch and Augustine 1998; Takechi et al. 1998; Barski et al. 2003). Amplitude and time-course of the Ca^{2+} transient

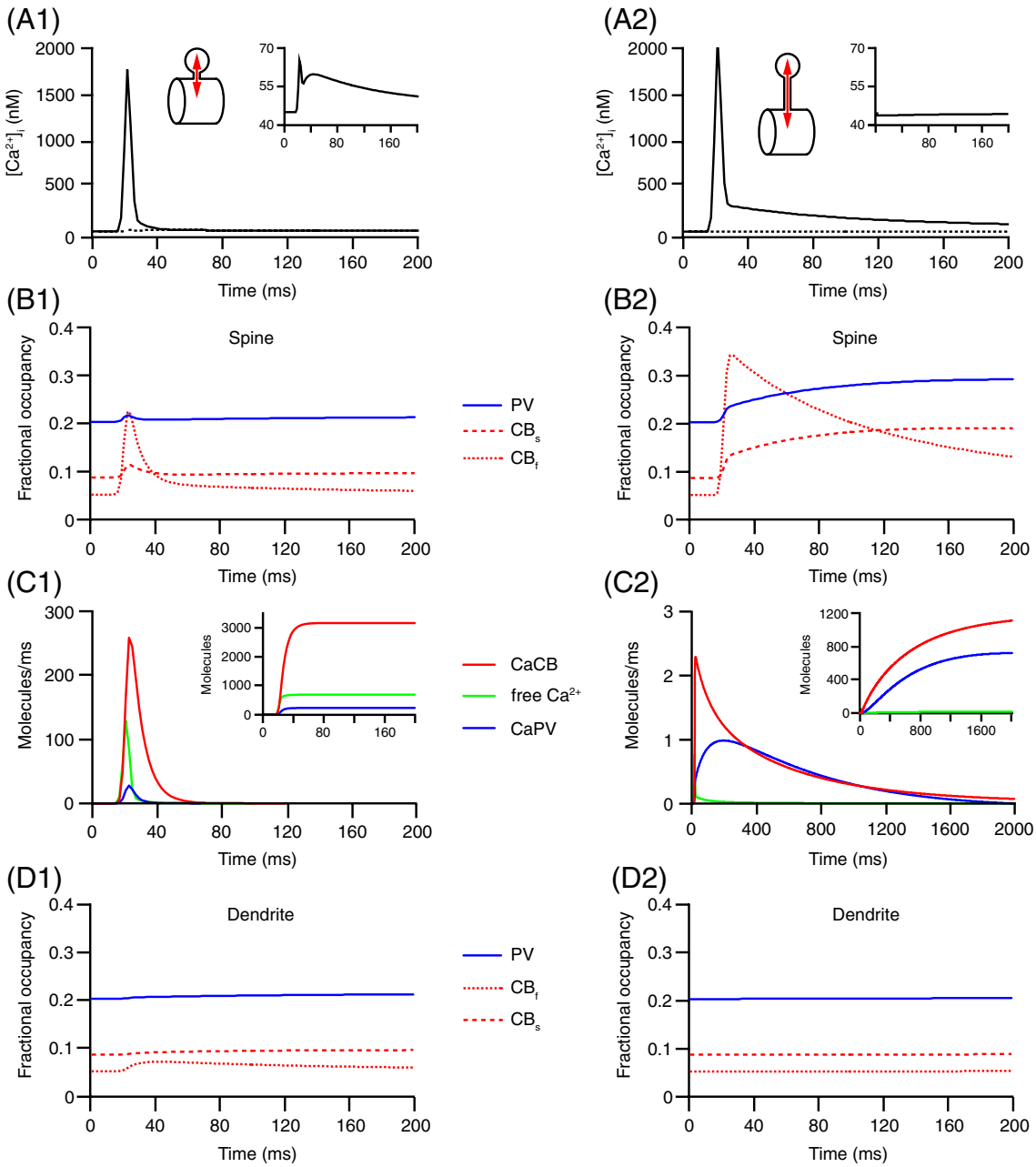

Fig. 3 Spino-dendritic coupling during rapid Ca^{2+} signaling for stubby and slim spines (*left and right column*, respectively) for unperturbed conditions, i.e., in the absence of indicator dye and without wash-out of CB and PV due to a prolonged whole-cell recording. (*A1*) Simulated rapid Ca^{2+} transient in spines with short thick necks ("stubby" spines) and their parent dendrites (*solid and dashed lines*, respectively). The *inset* show the increase in free Ca^{2+} ($[Ca^{2+}]_i$) in the inactive dendrite, which results from Ca^{2+} diffusion across the spine necks (see (*C1*)). The small initial peak of the dendritic Ca^{2+} transient relates to diffusion of free Ca^{2+}. (*B1*) Ca^{2+}-bound fractions of parvalbumin (PV, *blue*) and Calbindin (CB, *red*) in the spine during the Ca^{2+} transient. The fast and slow binding sites of CB (CB_f and CB_s, *dotted and dashed line*, respectively) are shown separately. (*C1*) Time course of net Ca^{2+} diffusion from the spine into the dendrite and its temporal integral (*inset*). Diffusion of free Ca^{2+} is shown in *green*, diffusion of Ca^{2+} bound to PV (CaPV) and to CB (CaCB) in *blue and red*, respectively. (*D1*) Same as in B1 but for the dendrite. (*A2–D2*) As in *A1–D1* but for a long thin spine neck geometry ("slim" spine). Note the changes in *x*- and *y*-scaling in (*C2*) compared to (*C1*)

were simulated according to the median of the experimental data on mGluR-mediated Ca^{2+} signals (see Fig. 2(d, f)).

In stubby spines (Fig. 4, left column), the Ca^{2+} transients reached a peak amplitude of ~200 nM and lasted about 3 s (Fig. 4(A1)). ~37.000 calcium ions entered the spine. The fast binding sites of CB could directly follow the Ca^{2+} transient while the kinetics of the slow binding sites of CB as well as those of PV lagged behind by ~1 s (Fig. 4(B1)). Overall, the change in the fractions of Ca^{2+}-bound buffers were moderate.

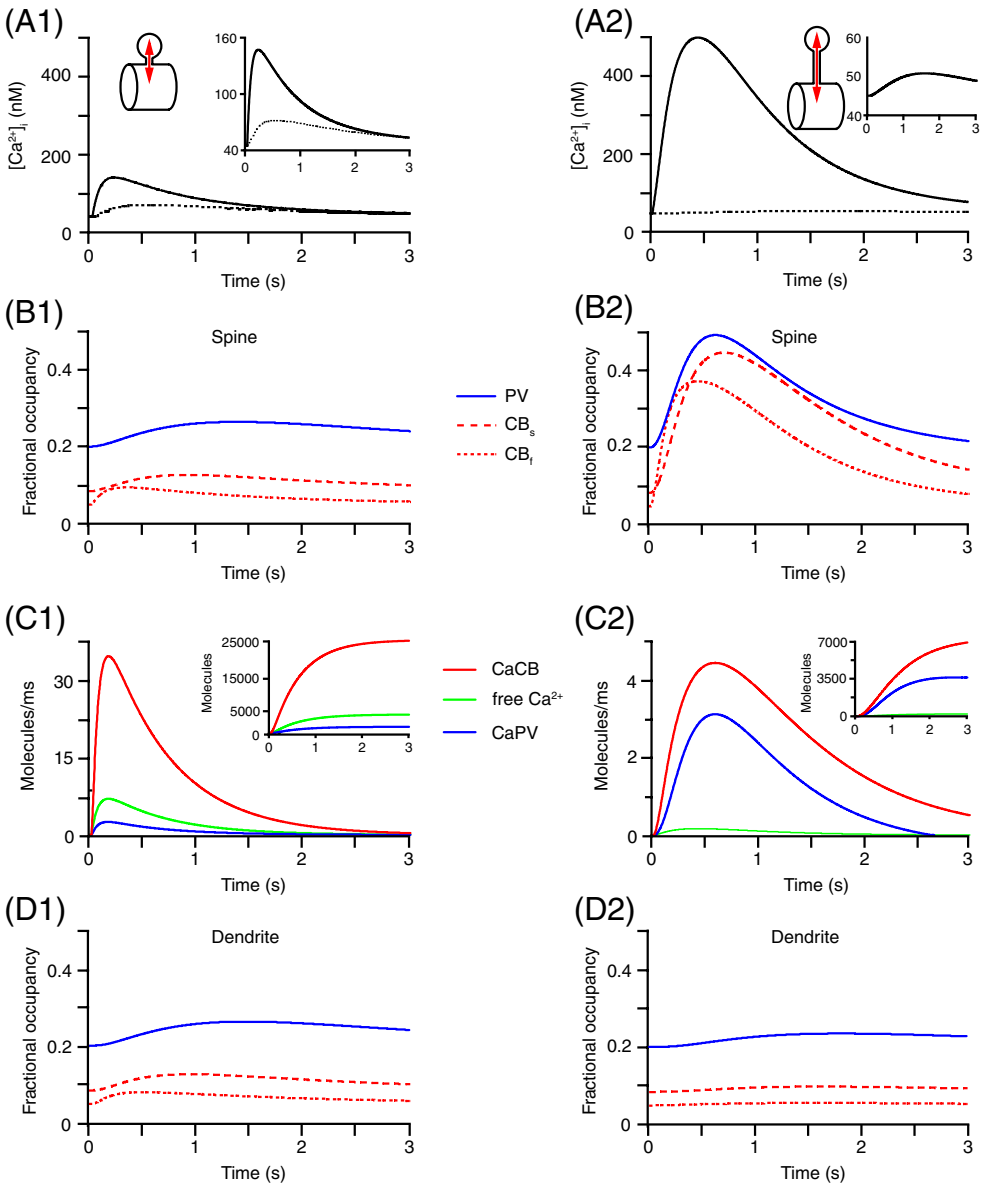

Fig. 4 Spino-dendritic coupling during slow Ca^{2+} signaling in stubby and slim spines (*left and right column*, respectively). (*A1–D2*) as in Fig. 3. Note the longer time course of the transients

More than 80% of the spineous Ca^{2+} load left the spine by diffusion, predominantly as Ca^{2+} bound to CB (70%) or as free Ca^{2+} (11%; Fig. 4(C1)). Diffusional flux of PV-bound Ca^{2+} was negligible (< 3%). Remarkably, the Ca^{2+} occupancy of PV and CB in the dendrite closely mirrored that in the spine (Fig. 4(D1)). The dendritic $[Ca^{2+}]_i$ reached ~75 nM, i.e., ~50% of the spineous peak amplitude (Fig. 4(A1) inset). This elevation declined only slowly with a slope of ~8 nM/s.

Changing the spine neck geometry from stubby to slim strongly affected the slow Ca^{2+} transient and the diffusional flux (Fig. 4(A2)). The amplitude of the spineous $[Ca^{2+}]_i$ increased to about 500 nM (i.e., three to four times larger than in the stubby spine) and its decay was significantly prolonged, which agrees with the above findings for rapid signaling. In the spine, CB and PV effectively buffered the Ca^{2+} transient. All buffer species could closely follow the transient (Fig. 4(B2)) without saturation (defined here as exceeding a fractional occupancy of 0.5; Schmidt et al. 2003a). Interestingly, for these long lasting signals, the slow, high-affinity binding sites (PV and CB_{slow}) outcompeted the fast, medium-affinity sites of CB (CB_{fast}). Despite the large and prolonged increases in $[Ca^{2+}]_i$ and in Ca^{2+}-buffer complexes, the diffusional flux of these species towards the dendrite was severely limited by the spine neck. Overall, the flux was three-fold decreased, carrying less than 30% of the total spineous Ca^{2+} load into the dendrite (Fig. 4(C2)). Consistently, the fractional occupancy of CB and PV were basically unaffected in the dendrite (Fig. 4(D2)) and the dendritic $[Ca^{2+}]_i$ increased only by ~5 nM (Fig. 4(A2) inset).

We again assessed the amount of compartmentalization by prohibiting diffusion between spine and dendrite (data not shown). Under this condition, the spineous Ca^{2+} transient as well the Ca^{2+} occupancy of CB and PV largely resembled those in the spines coupled to the dendrite by a slim neck. This underlines the above notion that a long and thin neck is effective in sequestering Ca^{2+} in the spine, even during long-lasting signals.

3.5 Effects of spine neck geometry on Ca^{2+}-dependent downstream signaling

In a final set of simulations we analyzed the functional consequences of the Ca^{2+} handling in stubby and slim spines by including the ubiquitous Ca^{2+} sensor calmodulin (CaM) in the model. CaM is activated by binding to Ca^{2+} and triggers a variety of downstream cascades that regulate fundamental cellular processes like survival, gene expression and synaptic plasticity (Xia and Storm 2005). Figure 5 illustrates the relative increases in Ca^{2+}–CaM complexes (CaM*) over baseline complex concentration ($\Delta CaM^*/CaM_0^*$) during rapid and slow synaptic Ca^{2+} signaling and the corresponding temporal integrals (insets). In stubby spines, total CaM activation was negligible during rapid signaling (Fig. 5(A1)) but substantially increased during slow signaling (Fig. 5(A2)). This is in agreement with previous findings in pyramidal neurons (Sabatini et al. 2002) and PNs (Schmidt et al. 2007), showing that sustained Ca^{2+} increases are required for CaM activation. As a consequence of the strong diffusional coupling, CaM* in the inactive dendrite reached approximately half of the value in the adjacent spine during the slow Ca^{2+} signal, an effect that could either result from diffusion of CaM* or of diffusion of free and/or bound Ca^{2+} across the spine neck. To distinguish between these two possibilities, we immobilized all species but CaM and CaM* in our simulations. Consistent with our previous findings (Schmidt et al. 2007), this abolished the dendritic increase in CaM* (data not shown), demonstrating that the main source of dendritic CaM activation is the spineous Ca^{2+} efflux and not diffusion of CaM*.

In slim spines, the active CaM reached significantly higher values. Already during brief signals (Fig. 5(B1)) the CaM* level was comparable to that in stubby spines during slow signals. The effects of biochemical compartmentalization were even more dramatic during slow Ca^{2+} signaling (Fig. 5(B2)) during which the integral of the spineous CaM activation was >5 times larger than in stubby spines while the dendritic CaM* remained unaffected.

4 Discussion

Numerical computer simulations, largely constrained by experimental data, were used to analyze the impact of the spine neck geometry on buffered Ca^{2+} diffusion from

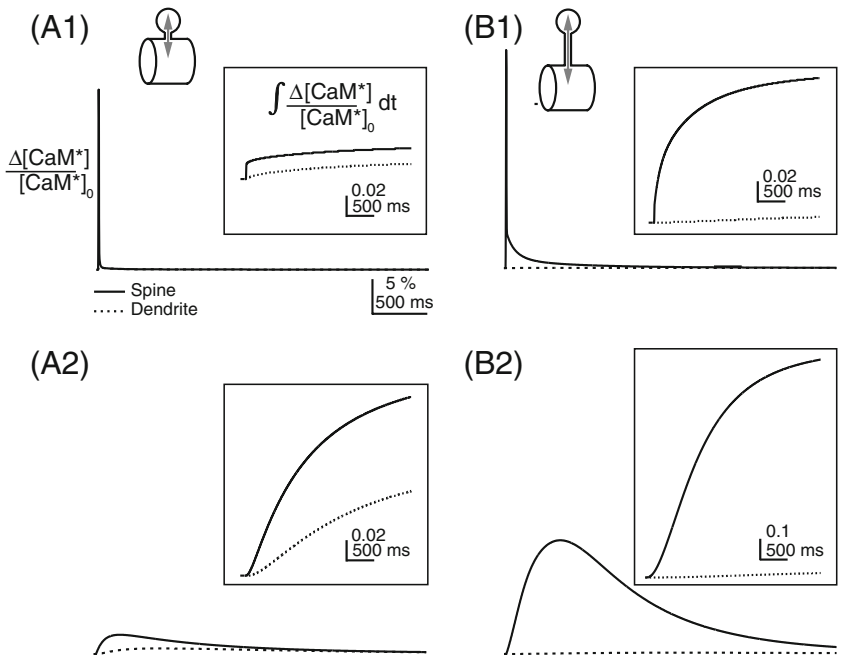

Fig. 5 Calmodulin (CaM) activation during spineous Ca^{2+} transients. (*A1*) Increases in Ca^{2+}-calmodulin complexes (activated CaM, CaM*) normalized to the resting activation ($\Delta CaM^*/CaM_0^*$) during rapid Ca^{2+} signaling in stubby spines (*solid lines*) and the parent dendrites (*dashes lines*). (*A2*) As in (*A1*) but for slow spineous Ca^{2+} signals. (*B1*, *B2*) As in (*A1*) and (*A2*) but for slim spines. The *insets* show the normalized temporal integral of CaM*; note that the change in *x*- and *y*-scaling in the *inset* to (*A2*)

spines into dendrites and on subsequent Ca^{2+}-dependent dendritic downstream signaling. Recently, it was shown (Schmidt et al. 2007) that mobile endogenous calbindin-D28k (CB) and parvalbumin (PV) transport the major fraction of Ca^{2+} (~ 75%) entering a spine of average morphology during synaptic activation into the parent dendrite. The present simulations suggest, that the spine neck is a potent regulator of this buffered Ca^{2+} efflux ranging form ~30% of the total Ca^{2+} load in slim spines to >80% in stubby spines (Fig. 6). Thus, subsequent Ca^{2+}-dependent calmodulin (CaM) activation was isolated in slim spines but closely linked to the dendrite in stubby spines (Fig. 5), at least when neighboring spines are coactive.

We simulated the equivalence of activation of multiple, neighboring spines without co-activation of dendritic voltage-gated Ca^{2+} channels (VOCCs; Denk et al. 1995). This form of synaptic activity plays a role in experimentally induced forms of synaptic plasticity (for review, see Daniel et al. 1998), as do forms of activity that recruit dendritic VOCCs (Eilers et al. 1995, 1997). For the latter, spino-dendritic coupling will play a less significant role because of the reduced net flux between the two coactive compartments (Schmidt et al. 2007). Activation of dendritic VOCCs requires that the synaptic excitation reaches a certain voltage threshold (Eilers et al. 1995). Thus, our simulations represent a degree of synaptic activation (Denk et al. 1995) that may merge seamlessly with conditions of stronger synaptic drive (Eilers et al. 1995, 1997).

The present work did not cover the topic of Ca^{2+} microdomain formation, which would require spatially resolved modelling. During spine activation, such microdomains develop within the spine neck (Holcman et al. 2004) or at its exit (Blackwell et al. 2006; Schmidt et al. 2007). Microdomains have a significant impact on neuronal information processing, at post- as well as at presynaptic sites (Augustine et al. 2003). In the case of activation of a single or a few spines, they may become relevant dendritic signaling domains because of the rapid dilution of Ca^{2+} in the large dendritic volume (Blackwell 2006, Schmidt et al. 2007). However, more detailed information about the localization of Ca^{2+}-dependent downstream processes in PNs would be required to quantify differences between local and global effector activation.

A direct observation of buffered Ca^{2+} diffusion is at present not possible. Ca^{2+} indicator dyes are themselves mobile buffers and their use inevitably distorts the spatio-temporal extend of Ca^{2+} signals (Neher 1999; Sabatini et al. 2002). Distortion-free measurements would require, for example, genetically-encoded, CB/PV-based reporter proteins similar to troponin C-based Ca^{2+} sensors (Heim and Griesbeck 2004; Heim et al. 2007) or indicators that work as collisional quenchers, not Ca^{2+} chelators. As long as

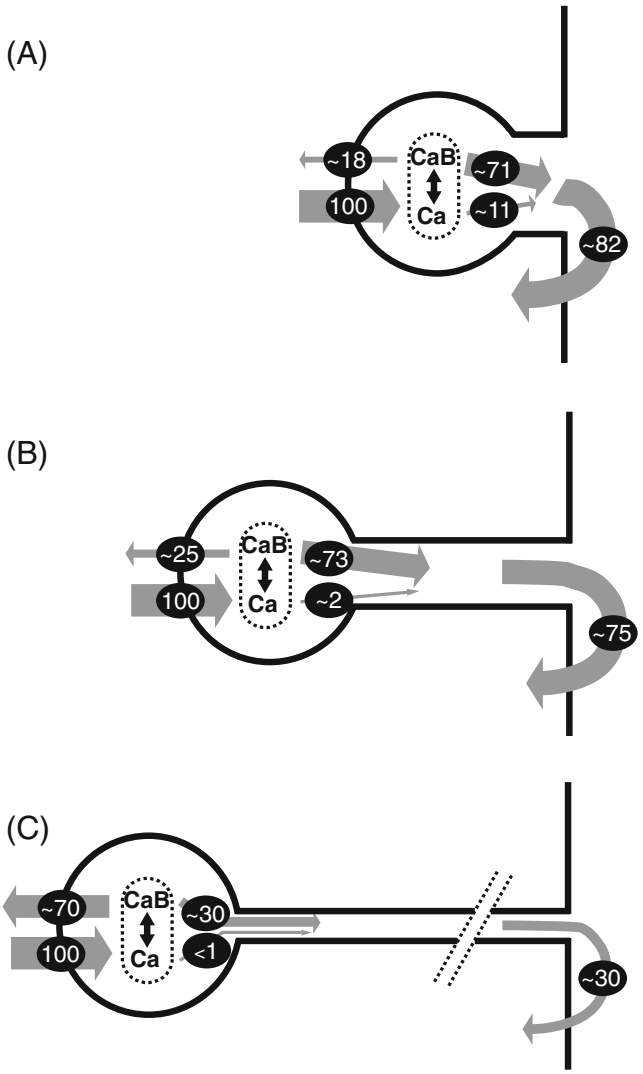

Fig. 6 Summary of neck impact on spino-dendritic cross-talk. (**a**) Reactions and diffusion of Ca^{2+} (Ca) entering a stubby spine. The *numbers* represent percent values interpolated between slow and fast Ca^{2+} signals. The majority of the Ca^{2+} is rapidly bound to buffers (CaB) and undergoes buffered diffusion towards the dendrite (~71%). In addition, ~11% of the spineous Ca^{2+} load diffuses unbuffered into the dendritic compartment from where it is subsequently cleared by dendritic extrusion mechanisms. Only ~18% of the spineous Ca^{2+} is cleared directly from the spine. (**b**, **c**) Same as in (**a**) but for a median (**b**) and a slim spine (**c**), respectively. Data shown in (**b**) are from Schmidt et al. (2007). The length of the spine neck is not drawn to scale in **c** (indicated by the *dashed lines*)

such sensors remain unavailable, studies on buffered diffusion will have to rely on indirect methods like computer simulations, which should be thoroughly tested on experimental data. Thus, a major aspect of our model is that only two of >40 parameters were variable during model adjustment. All other parameters were taken from experiments and kept invariant (see Appendix).

In recent years evidence has been accumulated that action potential-evoked Ca^{2+} transients in dendrites and spines decay rapidly, with time constants well below

100 ms. Such rapid Ca^{2+} kinetics were reported in brain slices and *in vivo* in CA1 and neocortical pyramidal neurons as well as for cerebellar PNs (Yuste and Denk 1995; Sabatini et al. 2002; Noguchi et al. 2005; Markram et al. 1995; Helmchen et al. 1996; Svoboda et al. 1997; Denk et al. 1995; Eilers et al. 1995; Schmidt et al. 2003a). During these short-lived signals Ca^{2+} will not be in equilibrium with its reaction partners: Binding sites with rapid on-rates will be occupied stronger than assumed from simulations based on equilibrium constants and slower binding sites will be less occupied (Markram et al. 1998; Schmidt et al. 2003a; Hernjak et al. 2005; Schmidt et al. 2007). We therefore used a kinetic model based on ordinary differential equations (ODEs) to simulate diffusional coupling between spines and dendrites. ODEs yielded rapid computation times even for long-lasting Ca^{2+} signals, which was a prerequisite for fitting the model to our experimental data.

The following assumptions underlay ODE-based models: First, the system is well mixed (spatially homogenous) and second, the system is deterministic, i.e., the evolution of the system is determined by the initial conditions. The first assumption is likely to be fulfilled since in PNs, which have a high Ca^{2+} buffering capacity (Fierro and Llano 1996), several thousands of molecules (buffers and Ca^{2+}) are located within small volumes (Kosaka et al. 1993; Maeda et al. 1999). Given the large numbers of reactants and assuming a non-chaotic behavior of the system, the solutions of stochastic models fluctuate around the deterministic solution, although the outcome of individual trials can significantly deviate from it (Rao et al. 2002; Bhalla 2004a; Blackwell 2006; Mayawala et al. 2006). Furthermore, the two compartments we modeled represent the resolvable structures from which volume-averaged fluorescence signals were recorded during line-scan imaging (Schmidt et al. 2003a, 2007). Finally, we previously showed that, as long as detailed information on the localization of the Ca^{2+}-dependent downstream signaling processes are unavailable, a two-compartment and a spatially resolved, finite element model yield strongly overlapping results (Schmidt et al. 2007). It should be noted that this might be different in cells with a low concentration of endogenous CaBPs, as e.g. pyramidal neurons. For such cells, stochastic modeling may be more adequate (Franks and Sejnowski 2002; Bhalla 2004a, b, Keller et al. 2008). The second assumption ("the system is deterministic") is likely to hold during rapid Ca^{2+} signaling, which is relatively invariant for a given recording site (Schmidt et al. 2003a). The low trial to trial variability demonstrates their deterministic character. Yet it may not hold for the slow Ca^{2+} signals. Here, we observed a larger trial to trial variability, possibly due to the involvement of second messenger cascades (Bhalla 2004b). However, we did not model the complete second messenger cascade leading to variability but focused on the median signal (Fig. 2(F)). Thus, neglecting the variance, our model likely provides a reliable picture of the average Ca^{2+} transient.

It is important to note that the observed effects on Ca^{2+} transport were mediated by the interplay of the neck geometry with CB and PV and vanished if the endogenous CaBPs were assumed to be immobile. This requires a substantial concentration of endogenous CaBPs, as present in cerebellar PNs (Kosaka et al. 1993; Maeda et al. 1999). The concentration of CaBPs can be quantified by the endogenous buffer capacitance (κ_s; Neher and Augustine 1992), which ranges from 900 to 2000 (Fierro and Llano 1996) in PNs. In pyramidal neurons or interneurons, however, κ_s values of only 20 to 90 were reported (Helmchen et al. 1996; Lee et al. 2000b; Kaiser et al. 2001; Sabatini et al. 2002; Noguchi et al. 2005). Thus, our observations may only apply to highly buffered cells like PNs. Indeed, one view of pyramidal spines is that they represent isolated Ca^{2+} signaling compartments with negligible Ca^{2+} diffusion into the dendrite (Gamble and Koch 1987; Zador et al. 1990; Guthrie et al. 1991; Müller and Connor 1991; Koch and Zador 1993; Svoboda et al. 1996; Sabatini et al. 2002). In a contrasting view, however, also the latter spines were subdivided into two classes depending on whether Ca^{2+} efflux into the dendrite contributed to the spine Ca^{2+}-decay kinetics or not (Volfovsky et al. 1999; Majewska et al. 2000a, b; Holthoff et al. 2002; Noguchi et al. 2005). Given the low κ_s value of pyramidal neurons, spineos Ca^{2+} efflux into the dendrite would require a stronger contribution of diffusion of free Ca^{2+}. Despite the fact that experimental observations on Ca^{2+} diffusion will be biased by the use of fast-on rate indicator dyes (Neher 1999; Sabatini et al. 2002) a simple explanation for the above ambiguity could arise from differences in the spine populations investigated (reviewed in Hayashi and Majewska 2005). Interestingly, we find that slim necks cause a substantial degree of Ca^{2+} compartmentalization even in the presence of CB and PV while spines with short necks show an intense spino-dendritic coupling and that the contribution of free Ca^{2+} diffusion increases significantly in stubby spines. On the other hand, apparent compartmentalization can also result from the large spino-dendritic volume difference, particularly during short-lived Ca^{2+} signals (Blackwell 2006; Schmidt et al. 2007).

A consequence of differential Ca^{2+} handling in stubby and slim spines is not only that the spineous Ca^{2+} decay kinetics were different (Figs. 3(A), 4(A)) but also that slow CaBPs and thus also slow Ca^{2+} sensors are preferentially activated in slim spines (Figs. 3(B), 4(B)). A possible sensor candidate protein is CB, which has two to three slow binding sites (Nägerl et al. 2000) and acts as a regulator of the IP3 signaling cascade (Berggård et al. 2002; Schmidt et al. 2005).

The focus of the present study was on postsynaptic information integration, which is classically viewed as the spatio-temporal summation of synaptic potentials in dendrites and subsequently at the axon hillock, followed by an all-or-none output signal if the membrane potential reaches threshold. There is ongoing debate whether the spine-neck resistance is sufficiently large to influence this electrical integration process (Koch and Zador 1993; Svoboda et al. 1996; Tsay and Yuste 2004; Araya et al. 2006). Our simulations suggest that the neck resistance has at least a profound impact on biochemical dendritic signal integration. For these effects to occur, co-activation of neighboring spines at a density of at least three to four spines was simulated here, according to the observed density of distal spines in PNs (Vecellio et al. 2000). This is similar to the spine densities in adult hippocampal CA1 pyramidal cells and hippocampal granule cells, where estimates range from 2 to 4 spines per µm. These estimates stem from serial section electron microscopy, which yielded even higher densities in PNs of up to 10 spines per µm (reviewed in Nimchinsky et al. 2002). Thus, while our simulations likely give a lower boundary of biochemical dendritic integration in PNs, they may, to a certain extent, also reflect the situation in other spiny neurons.

Spino-dendritic coupling may be further enhanced by activity-dependent twitching of spines, which occurs in the hippocampus on the timescale of synaptic calcium transients (Korkotian and Segal 2001). While Purkinje cell spines are in general as motile as those of hippocampal neurons (Dunaevsky et al. 1999), it remains to be clarified whether they also undergo rapid, Ca^{2+}-dependent twitching. Depending on the degree of morphological changes, the accompanied outflow of spineous cytosol may significantly boost spino-dendritic coupling (Holcman et al. 2004).

In close analogy to Allbritton et al. (1992), the range of action of dendritic buffer-bound Ca^{2+} can be estimated to be $(2\ D\ \tau)^{1/2}$, where D is the diffusion coefficient of the buffer and τ the inverse of the off rate of the Ca^{2+}/buffer complex. Assuming normal diffusion within the dendrite, Ca^{2+} bound to PV, CaM and the medium- and high-affinity binding sites of CB could act on ranges of 10, 0.1, 3, and 1 µm, respectively. However, the values for PV and, to lesser extend, for CB represent upper bounds because spines will significantly retard diffusion within the dendrite (Santamaria et al. 2006). In view of the fact that PV showed a negligible Ca^{2+} occupation in dendrites in all simulations, the average range of action of buffer-bound Ca^{2+} will only be ~2 µm. This low number is in agreement with previous work on dendritic Ca^{+} signaling in cerebellar Purkinje neurons (Eilers et al. 1995, 1997) that showed a steep gradient between active and inactive dendritic branches. Spino-dendritic coupling, therefore, may unite spines and their adjacent dendritic compartments to small signaling units that are decoupled from neighboring inactive spiny branchlets.

Acknowledgements We thank Stefan Hallermann for critical discussion and Gudrun Bethge for technical assistance. The work was supported by grants from the Bundesministerium für Bildung und Forschung to J.E.

Appendix

Table 1 Values and Parameters of the Simulation

Parameter	Value	Notes
$[Ca^{2+}]_{rest}$	45 nM	Wilms et al. (2006)
$[Mg^{2+}]_i$	590 µM	Calculated, held constant
Spine Ca^{2+} current		
CF-mediated		
Peak amplitude	36 pA	
Width	4 ms	
mGluR-mediated		
Peak amplitude	28 pA	
Apparent τ_{rise}, τ_{decay}	60, 600 ms	
Total Ca^{2+} influx		
CF signal		
Spine	~4,700 ions	For the median response
Dendrite	~35,000/−ions	No influx in the simulations
mGluR-mediated signal		
Spine	~37,000 ions	For the median response
Dendrite	~ 148,000/−ions	No influx in the simulations
Extrusion		
Michaelis–Menten constant, K_M	3 µM	
Maximal pump velocity, v_{max}	30–300 pmol cm^{-2} s^{-1}	
Oregon Green BAPTA-1		
Effective concentration	160 or 80 µM	80% of pipette conc.
K_D	325 nM	Schmidt et al. (2003a)
k_{off}	140 s^{-1}	Eberhard and Erne (1991)[a]
k_{on}	430 μM^{-1} s^{-1}	Calculated
Calbindin D_{28k}		
Effective concentration	120 µM	Kosaka et al. (1993)[b]
After correction for wash-out	50 µM	–[c]
Binding sites (non-cooperative)	4	Nägerl et al. (2000)

Table 1 (continued)

Parameter	Value	Notes
Ratio of high- to medium-affinity binding sites	2:2	Ibid.
$k_{off,\ medium\ aff.}$	35.8 s^{-1}	Ibid.
$k_{off,\ high\ aff.}$	2.6 s^{-1}	Ibid.
$k_{on,\ medium\ aff.}$	43.5 $\mu M^{-1}\ s^{-1}$	Ibid. and [d]
$k_{on,\ high\ aff.}$	5.5 $\mu M^{-1}\ s^{-1}$	Ibid. and [d]
$K_{D,\ medium\ aff.}$	822 nM	Calculated
$K_{D,\ high\ aff.}$	474 nM	Calculated
Parvalbumin		
Effective concentration	75 μM	Kosaka et al. (1993)
After correction for wash-out	40 μM	–[c]
Binding sites (non-cooperative)	2	Eberhard and Erne (1994)
$k_{off,Ca}$	0.95 s^{-1}	Lee et al. (2000a)
$k_{off,Mg}$	25 s^{-1}	Ibid.
$K_{D,Ca}$	9 nM	Ibid.
$K_{D,Mg}$	31 μM	Eberhard and Erne (1994)
$k_{on,Ca}$	107 $\mu M^{-1}\ s^{-1}$	Calculated
$k_{on,Mg}$	0.8 $\mu M^{-1}\ s^{-1}$	Calculated
Calmodulin		
Effective concentration	10 μM	Estimated from Eberhard and Erne (1991)
Binding sites	1	From the four sites only the first, rate-limiting one was considered
k_{off}	2.200 s^{-1}	–[e]
K_D	55 μM	Ibid.
k_{on}	40 $\mu M^{-1}\ s^{-1}$	Ibid.
Geometry		
Volume of spine head	0.083 μm^3	Harris and Stevens (1988)
Surface area of spine head	0.9 μm^2	Ibid.
Radii and lengths of spine necks		Ibid.
Stubby spine	0.15 and 0.12 μm	
Average spine	0.09 and 0.66 μm	
Slim spine	0.045 and 2.18 μm	
Spine density	3.4 μm^{-1}	Vecellio et al. (2000)
Radius of dendritic segment	1 μm	
Length of dendritic segment	0.3 μm	Calculated from spine density

Table 1 (continued)

Parameter	Value	Notes
Diffusional mobility		
D_{Ca}	223 $\mu m^2\ s^{-1}$	Allbritton et al. (1992)
D_{OGB}	15 $\mu m^2\ s^{-1}$	Holthoff et al. (2002) and [a]
D_{PV}	43 $\mu m^2\ s^{-1}$	Schmidt et al. (2003b)
D_{CB}	20 $\mu m^2\ s^{-1}$	Schmidt et al. (2005)
D_{CaM}	21 $\mu m^2\ s^{-1}$	Schmidt et al. (2007)
Fraction of immobile CB	0.2	Schmidt et al. (2005)
Fraction of immobile CaM	0.2	Schmidt et al. (2007)

[a] Data for Calcium Green 1, an indicator dye closely related to OGB

[b] Assuming that 33% of CB is occupied by Mg^{2+}

[c] Assuming a ~50% washout during our whole-cell recordings

[d] Assuming twofold slower kinetics in the cytosol compared to the *in vitro* data (Berggård et al. 2002)

[e] Faas et al. (2004)

References

Allbritton, N. L., Meyer, T., & Stryer, L. (1992). Range of messenger action of calcium ion and inositol 1,4,5-trisphosphate. *Science*, *258*, 1812–1815. doi:10.1126/science.1465619.

Araya, R., Jiang, J., Eisenthal, K. B., & Yuste, R. (2006). The spine neck filters membrane potentials. *Proceedings of the National Academy of Sciences of the United States of America*, *103*, 17961–17966. doi:10.1073/pnas.0608755103.

Augustine, G. J., Santamaria, F., & Tanaka, K. (2003). Local calcium signaling in neurons. *Neuron*, *40*, 331–346. doi:10.1016/S0896-6273(03)00639-1.

Barski, J. J., Hartmann, J., Rose, C. R., Hoebeek, F., Mörl, K., Noll-Hussong, M., et al. (2003). Calbindin in cerebellar Purkinje cells is a critical determinant of the precision of motor coordination. *The Journal of Neuroscience*, *23*, 3469–3477.

Berggård, T., Szczepankiewicz, O., Thulin, E., & Linse, S. (2002). Myo-inositol monophosphatase is an activated target of calbindin D28k. *The Journal of Biological Chemistry*, *277*, 41954–41959. doi:10.1074/jbc.M203492200.

Bhalla, U. S. (2004a). Signaling in small subcellular volumes. I. Stochastic and diffusion effects on individual pathways. *Biophysical Journal*, *87*, 733–744. doi:10.1529/biophysj.104. 040469.

Bhalla, U. S. (2004b). Signaling in small subcellular volumes. II. Stochastic and diffusion effects on synaptic network properties. *Biophysical Journal*, *87*, 745–753. doi:10.1529/biophysj.104.040501.

Blackwell, K. T. (2006). An efficient stochastic diffusion algorithm for modeling second messengers in dendrites and spines. *Journal of Neuroscience Methods*, *157*, 142–153. doi:10.1016/j.jneumeth.2006.04.003.

Bloodgood, B. L., & Sabatini, B. L. (2005). Neuronal activity regulates diffusion across the neck of dendritic spines. *Science*, *310*, 866–869. doi:10.1126/science.1114816.

Bonhoeffer, T., & Yuste, R. (2002). Spine motility. Phenomenology, mechanisms, and function. *Neuron*, *35*, 1019–1027. doi:10.1016/S0896-6273(02)00906-6.

Crick, F. (1982). Do dendritic spines twitch? *Trends in Neurosciences*, *5*, 44–46. doi:10.1016/0166-2236(82)90020-0.

Daniel, H., Levenes, C., & Crepél, F. (1998). Cellular mechanisms of cerebellar LTD. *Trends in Neurosciences*, *21*, 401–407. doi:10.1016/S0166-2236(98)01304-6.

Denk, W., Sugimori, M., & Llinás, R. (1995). Two types of calcium responses limited to single spines in cerebellar Purkinje cells. *Proceedings of the National Academy of Sciences of the United States of America*, *92*, 8279–8282. doi:10.1073/pnas.92.18.8279.

Dunaevsky, A., Tashiro, A., Majewska, A., Mason, C., & Yuste, R. (1999). Developmental regulation of spine motility in the mammalian central nervous system. *Proceedings of the National Academy of Sciences of the United States of America*, *96*, 13438–13443. doi:10.1073/pnas.96.23.13438.

Eberhard, M., & Erne, P. (1991). Calcium binding to fluorescent calcium indicators : calcium green, calcium orange and calcium crimson. *Biochemical and Biophysical Research Communications*, *180*, 209–215. doi:10.1016/S0006-291X(05)81278-1.

Eberhard, M., & Erne, P. (1994). Calcium and magnesium binding to rat parvalbumin. *European Journal of Biochemistry*, *222*, 21–26. doi:10.1111/j.1432-1033.1994.tb18836.x.

Eilers, J., Augustine, G. J., & Konnerth, A. (1995). Subthreshold synaptic Ca^{2+} signalling in fine dendrites and spines of cerebellar Purkinje neurons. *Nature*, *373*, 155–158. doi:10.1038/373155a0.

Eilers, J., Takechi, H., Finch, E. A., Augustine, G. J., & Konnerth, A. (1997). Local dendritic Ca^{2+} signaling induces cerebellar LTD. *Learning & Memory (Cold Spring Harbor, N.Y.)*, *3*, 159–168. doi:10.1101/lm.4.1.159.

Faas et al. (2004), Soc. Neurosci. Abstr. No 165.5.

Fiala, J. C., & Harris, K. M. (2005). Dendrite Structure. In G. Stuart, N. Spruston, & M. Häusser (Eds.), *Dendrites* (pp. 1–34). Oxford: Oxford University Press.

Fierro, L., & Llano, I. (1996). High endogenous calcium buffering in Purkinje cells from rat cerebellar slices. *The Journal of Physiology*, *496*, 617–625.

Finch, E. A., & Augustine, G. J. (1998). Local calcium signalling by inositol-1,4,5-trisphosphate in Purkinje cell dendrites. *Nature*, *396*, 753–756. doi:10.1038/25541.

Fischer, M., Kaech, S., Knutti, D., & Matus, A. (1998). Rapid actin-based plasticity in dendritic spines. *Neuron*, *20*, 847–854. doi:10.1016/S0896-6273(00)80467-5.

Franks, K. M., & Sejnowski, T. J. (2002). Complexity of calcium signaling in synaptic spines. *BioEssays*, *24*, 1130–1144. doi:10.1002/bies.10193.

Gamble, E., & Koch, C. (1987). The dynamics of free calcium in dendritic spines in response to repetitive synaptic input. *Science*, *236*, 1131–1135. doi:10.1126/science.3495885.

Guthrie, P. B., Segal, M., & Kater, S. B. (1991). Independent regulation of calcium revealed by imaging dendritic spines. *Nature*, *354*, 76–80. doi:10.1038/354076a0.

Harris, K. M., & Stevens, J. K. (1988). Dendritic spines of rat cerebellar Purkinje cells: serial electron microscopy with reference to their biophysical characteristics. *The Journal of Neuroscience*, *8*, 4455–4469.

Hartmann, J., & Konnerth, A. (2005). Determinants of postsynaptic Ca^{2+} signaling in Purkinje neurons. *Cell Calcium*, *37*, 459–466. doi:10.1016/j.ceca.2005.01.014.

Hayashi, Y., & Majewska, A. K. (2005). Dendritic spine geometry: Functional implication and regulation. *Neuron*, *46*, 529–532. doi:10.1016/j.neuron.2005.05.006.

Heim, N., & Griesbeck, O. (2004). Genetically encoded indicators of cellular calcium dynamics based on troponin C and green fluorescent protein. *The Journal of Biological Chemistry*, *279*, 14280–14286. doi:10.1074/jbc.M312751200.

Heim, N., Garaschuk, O., Friedrich, M. W., Mank, M., Milos, R. I., Kovalchuk, Y., et al. (2007). Improved calcium imaging in transgenic mice expressing a troponin C-based biosensor. *Nature Methods*, *4*, 127–129. doi:10.1038/nmeth1009.

Helmchen, F., Imoto, K., & Sakmann, B. (1996). Ca^{2+} buffering and action potential-evoked Ca^{2+} signaling in dendrites of pyramidal neurones. *Biophysical Journal*, *70*, 1069–1081. doi:10.1016/S0006-3495(96)79653-4.

Hernjak, N., Slepchenko, B. M., Fernald, K., Fink, C. C., Fortin, D., Moraru, I., et al. (2005). Modeling and analysis of calcium signaling events leading to long-term depression in cerebellar Purkinje cells. *Biophysical Journal*, *89*, 3790–3806. doi:10.1529/biophysj.105.065771.

Holcman, D., Schuss, Z., & Korkotian, E. (2004). Calcium dynamics in dendritic spines and spine motility. *Biophysical Journal*, *87*, 81–91. doi:10.1529/biophysj.103.035972.

Holthoff, K., Tsay, D., & Yuste, R. (2002). Calcium dynamics of spines depend on their dendritic location. *Neuron*, *33*, 425–437. doi:10.1016/S0896-6273(02)00576-7.

Kaiser, K. M., Zilberter, Y., & Sakmann, B. (2001). Back-propagating action potentials mediate calcium signalling in dendrites of bitufted interneurons in layer 2/3 of rat somatosensory cortex. *The Journal of Physiology*, *535*, 17–31. doi:10.1111/j.1469-7793.2001.t01-1-00017.x.

Keller, D. X., Franks, K. M., Bartol, T. M., & Sejnowski, T. J. (2008). Calmodulin activation by calcium transients in the postsynaptic density of dendritic spines. *PLoS ONE*, *3*, E2045. doi:10.1371/journal.pone.0002045.

Koch, C., & Zador, A. (1993). The function of dendritic spines: devices subserving biochemical rather than electrical compartmentalization. *The Journal of Neuroscience*, *13*, 413–422.

Korkotian, E., & Segal, M. (2001). Regulation of dendritic spine motility in cultured hippocampal neurons. *The Journal of Neuroscience*, *21*, 6115–6124.

Kosaka, T., Kosaka, K., Nakayama, T., Hunziker, W., & Heizmann, C. W. (1993). Axons and axon terminals of cerebellar Purkinje cells and basket cells have higher levels of parvalbumin immunoreactivity than somata and dendrites: quantitative analysis by immunogold labeling. *Experimental Brain Research*, *93*, 483–491. doi:10.1007/BF00229363.

Lee, S. - H., Schwaller, B., & Neher, E. (2000a). Kinetics of Ca^{2+} binding to parvalbumin in bovine chromaffin cells: Implications for $[Ca^{2+}]$ transients of neuronal dendrites. *The Journal of Physiology*, *525*, 419–432. doi:10.1111/j.1469-7793.2000.t01-2-00419.x.

Lee, S. - H., Rosenmund, C., Schwaller, B., & Neher, E. (2000b). Differences in Ca^{2+} buffering properties between excitatory and inhibitory hippocampal neurons from the rat. *The Journal of Physiology*, *525*, 405–418. doi:10.1111/j.1469-7793.2000.t01-3-00405.x.

Maeda, H., Ellis-Davies, G. C., Ito, K., Miyashita, Y., & Kasai, H. (1999). Supralinear Ca^{2+} signaling by cooperative and mobile Ca^{2+} buffering in Purkinje neurons. *Neuron*, *24*, 989–1002. doi:10.1016/S0896-6273(00)81045-4.

Majewska, A., Tashiro, A., & Yuste, R. (2000a). Regulation of spine calcium dynamics by rapid spine motility. *The Journal of Neuroscience*, *20*, 8262–8268.

Majewska, A., Brown, E., Ross, J., & Yuste, R. (2000b). Mechanisms of calcium decay kinetics in hippocampal spines: role of spine calcium pumps and calcium diffusion through the spine neck in biochemical compartmentalization. *The Journal of Neuroscience*, *20*, 1722–1734.

Markram, H., Helm, J., & Sakmann, B. (1995). Dendritic calcium transients evoked by single back-propagating action potentials in

rat neocortical pyramidal neurons. *The Journal of Physiology*, *485*, 1–20.

Markram, H., Roth, A., & Helmchen, F. (1998). Competitive calcium binding: implications for dendritic calcium signaling. *Journal of Computational Neuroscience*, *5*, 331–348. doi:10.1023/A:1008891229546.

Mayawala, K., Vlachos, D. G., & Edwards, J. S. (2006). Spatial modeling of dimerization reaction dynamics in the plasma membrane: Monte Carlo vs. continuum differential equations. *Biophysical Chemistry*, *121*, 194–208. doi:10.1016/j.bpc.2006.01.008.

Müller, W., & Connor, J. A. (1991). Dendritic spines as individual neuronal compartments for synaptic Ca^{2+} responses. *Nature*, *354*, 73–76. doi:10.1038/354073a0.

Müller, A., Kukley, M., Stausberg, P., Beck, H., Müller, W., & Dietrich, D. (2005). Endogenous Ca^{2+} buffer concentration and Ca^{2+} microdomains in hippocampal neurons. *The Journal of Neuroscience*, *25*, 558–565. doi:10.1523/JNEUROSCI.3799-04.2005.

Nägerl, U. V., Novo, D., Mody, I., & Vergara, J. L. (2000). Binding kinetics of calbindin-D_{28k} determined by flash photolysis of caged Ca^{2+}. *Biophysical Journal*, *79*, 3009–3018. doi:10.1016/S0006-3495(00)76537-4.

Neher, E. (1999). Some quantitative aspects of calcium fluorimetry. In R. Yuste, F. Lenny, & A. Konnerth (Eds.), *Imaging neurons: a laboratory manual* (pp. 31.31–31.11). New York: Cold Spring Harbor Laboratory Press.

Neher, E., & Augustine, G. J. (1992). Calcium gradients and buffers in bovine chromaffin cells. *The Journal of Physiology*, *450*, 273–301.

Nimchinsky, E. A., Sabatini, B. L., & Svoboda, K. (2002). Structure and function of dendritic spines. *Annual Review of Physiology*, *64*, 313–353. doi:10.1146/annurev.physiol.64.081501.160008.

Noguchi, J., Matsuzaki, M., Ellis-Davies, G. C., & Kasai, H. (2005). Spine-neck geometry determines NMDA receptor-dependent Ca^{2+} signaling in dendrites. *Neuron*, *46*, 609–622. doi:10.1016/j.neuron.2005.03.015.

Rao, C. V., Wolf, D. M., & Arkin, A. P. (2002). Control, exploitation and tolerance of intracellular noise. *Nature*, *420*, 231–237. doi:10.1038/nature01258.

Rexhausen, U. (1992). Bestimmung der Diffusionseigenschaften von Fluoreszenzfarbstoffen in verzweigten Nervenzellen unter Verwendung eines rechnergesteuerten Bildverarbeitungssystems. *University of Göttingen, Diploma thesis*.

Sabatini, B. L., Oertner, T. G., & Svoboda, K. (2002). The life cycle of Ca^{2+} ions in dendritic spines. *Neuron*, *33*, 439–452. doi:10.1016/S0896-6273(02)00573-1.

Santamaria, F., Wils, S., De Schutter, E., & Augustine, G. J. (2006). Anomalous diffusion in purkinje cell dendrites caused by spines. *Neuron*, *52*(4), 635–648. doi:10.1016/j.neuron.2006.10.025.

Schmidt, H., Stiefel, K., Racay, P., Schwaller, B., & Eilers, J. (2003a). Mutational analysis of dendritic Ca^{2+} kinetics in rodent Purkinje cells: role of parvalbumin and calbindin D_{28k}. *The Journal of Physiology*, *551*, 13–32. doi:10.1113/jphysiol.2002.035824.

Schmidt, H., Brown, E. B., Schwaller, B., & Eilers, J. (2003b). Diffusional mobility of parvalbumin in spiny dendrites of cerebellar Purkinje neurons quantified by fluorescence recovery after photobleaching. *Biophysical Journal*, *84*, 2599–2608. doi:10.1016/S0006-3495(03)75065-6.

Schmidt, H., Schwaller, B., & Eilers, J. (2005). Calbindin D28k targets *myo*-inositol monophosphatase in spines and dendrites of cerebellar Purkinje neurons. *Proceedings of the National Academy of Sciences of the United States of America*, *102*, 5850–5855. doi:10.1073/pnas.0407855102.

Schmidt, H., Kunerth, S., Wilms, C., Strotmann, R., & Eilers, J. (2007). Spino-dendritic cross-talk in rodent Purkinje neurons mediated by endogenous Ca^{2+}-binding proteins. *The Journal of Physiology*, *581*, 619–629. doi:10.1113/jphysiol.2007.127860.

Sjöström, P. J., Rancz, E. A., Roth, A., & Häusser, M. (2008). Dendritic excitability and synaptic plasticity. *Physiological Reviews*, *88*, 769–840. doi:10.1152/physrev.00016.2007.

Spacek, J., & Hartmann, M. (1983). Three-dimensional analysis of dendritic spines. I. Quantitative observations related to dendritic spine and synaptic morphology in cerebral and cerebellar cortices. *Anatomy and Embryology*, *167*, 289–310. doi:10.1007/BF00298517.

Svoboda, K., Tank, D. W., & Denk, W. (1996). Direct measurement of coupling between dendritic spines and shafts. *Science*, *272*, 716–719. doi:10.1126/science.272.5262.716.

Svoboda, K., Denk, W., Kleinfeld, D., & Tank, D. W. (1997). *In vivo* dendritic calcium dynamics in neocortical pyramidal neurons. *Nature*, *385*, 161–165. doi:10.1038/385161a0.

Takechi, H., Eilers, J., & Konnerth, A. (1998). A new class of synaptic responses involving calcium release in dendritic spines. *Nature*, *396*, 757–760. doi:10.1038/25547.

Tsay, D., & Yuste, R. (2004). On the electrical function of dendritic spines. *Trends in Neurosciences*, *27*, 77–83. doi:10.1016/j.tins.2003.11.008.

Vecellio, M., Schwaller, B., Meyer, M., Hunziker, W., & Celio, M. R. (2000). Alterations in Purkinje cell spines of calbindin D-28 k and parvalbumin knock-out mice. *The European Journal of Neuroscience*, *12*, 945–954. doi:10.1046/j.1460-9568.2000.00986.x.

Volfovsky, N., Parnas, H., Segal, M., & Korkotian, E. (1999). Geometry of dendritic spines affects calcium dynamics in hippocampal neurons: Theory and experiments. *Journal of Neurophysiology*, *82*, 450–462.

Wilms, C. D., Schmidt, H., & Eilers, J. (2006). Quantitative two-photon Ca^{2+} imaging via fluorescence lifetime analysis. *Cell Calcium*, *40*, 73–79. doi:10.1016/j.ceca.2006.03.006.

Xia, Z., & Storm, D. R. (2005). The role of calmodulin as a signal integrator for synaptic plasticity. *Nature Reviews. Neuroscience*, *6*, 267–276. doi:10.1038/nrn1647.

Yuste, R., & Denk, W. (1995). Dendritic spines as basic functional units of neuronal integration. *Nature*, *375*, 682–684. doi:10.1038/375682a0.

Zador, A., Koch, C., & Brown, T. H. (1990). Biophysical model of a Hebbian synapse. *Proceedings of the National Academy of Sciences of the United States of America*, *87*, 6718–6722. doi:10.1073/pnas.87.17.6718.